PCCP

PAPER

Hydrogen Bonding in Alkali Metal Cation-Bound i-Motif-Like Dimers of 1-Methyl Cytosine: An IRMPD Spectroscopic and Computational Study

Received 00th January 20xx,
Accepted 00th January 20xx

DOI: 10.1039/x0xx00000x

Ruodi Cheng,[a] Estelle Loire,[b] and Travis D. Fridgen[a,*]

The structures of alkali metal cation bound 1-methylcytosine (1-mCyt) dimers were explored using vibrational spectroscopy in the form of infrared multiple photon dissociation (IRMPD) spectroscopy and by computational methods. For the smaller alkali metal cations, Li^+ and Na^+, only non-hydrogen bonded symmetric anti-parallel structures were observed in agreement with the lowest energy computed structures. For K^+, Rb^+, and Cs^+ the vibrational spectra in the N-H stretch region showed strong evidence for hydrogen bonding in agreement with the lowest energy structures which contained hydrogen bonding interactions between the amine group of one cytosine and the carbonyl oxygen of the other cytosine. The lowest energy structures for these complexes were compared to previously studied cytosine complexes $[(Cyt)_2M]^+$ where M = Li, Na, and K. The calculations are in agreement that only the non-hydrogen bonded structures would be observed for these cytosine complexes.

1. Introduction

Large biomolecules, such as DNA can twist themselves into rather interesting self-assembled structures that are largely governed by intramolecular interactions within the molecule itself. Their structures are also affected by solvent molecules, other biomolecules, as well as the presence of metal cations. As the crucial part of G-quadruplex formation, the interactions and stabilization of G-quadruplexes by monovalent metal cations have been studied[1–4] since the discovery of G-tetrads in the sequence of human telomere *in vitro* in the 1980s.[2,5–8] The structures of, and intramolecular interactions within, G-quadruplexes are formed by folding in single strands or multi-strands of guanine-rich regions of DNA/RNA.[9–14] Alkali metal cations were found to stabilize the structure of the 9-ethylguanine (9eG) tetrad where Na^+ is greatly preferred over the other alkali metal cations in the solution phase.[15] A subsequent study conducted on gas-phase metal cationized tetrads[16] agreed with the stability ordering of the tetrads by alkali metal cations, $Na^+ > Li^+ > K^+$, Rb^+, Cs^+ determined in the solution phase. Studies on G-quadruplexes have concluded that stronger hydration of Na^+ compared to K^+ was responsible for the fact that it is K^+ that is associated with G-quadruplexes in biology.[17] However a study of gas-phase quadruplexes, $(9eG)_8M^+$, composed of two tetrads bound by Na^+, K^+, Rb^+, or Cs^+ revealed that *even in the absence of solvent* the quadruplex stabilized by K^+ is significantly more strongly bound than $(9eG)_8Na^+$, meaning that there is an intrinsic stability of the K^+-G-quadruplex[18] and shows the importance that gas-phase studies can have on the fundamental understanding of biomolecule interactions.

Similar to guanine, cytosine is a nucleobase in DNA and RNA which can form highly ordered structures. One such structure is called the i-motif which can be formed from four nucleic acid strands or by a single strand that can fold into four-stranded structures in cytosine rich regions.[19–22] While guanine quadruplexes are formed from tetrads, the i-motif is composed of pairs of cytosine protonated dimers; the guanine tetrad and protonated dimer of cytosine are shown in Scheme 1 a) and b), respectively. The i-motif is not particularly stable under basic physiological pH due to the requirement of protonation.[23] At

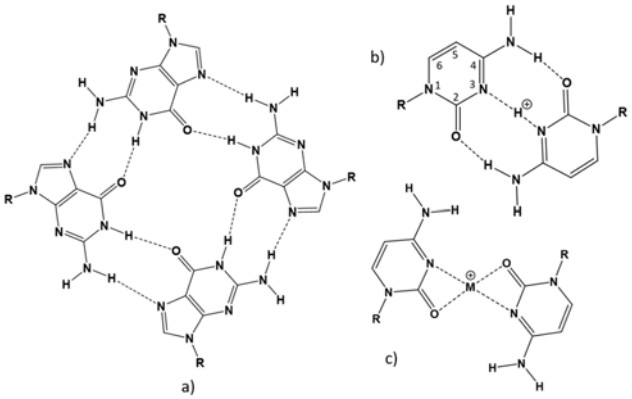

Scheme 1. Hydrogen bonding in a) the G-quadruplex and b) the i-motif. c) The reported symmetric anti-parallel (SAP) structure of the alkali metal cation bound dimer of cytosine, $(Cyt)_2M^+$, M=Li, Na, and K. The conventional ring numbering for cytosine is shown in b).

[a] *Department of Chemistry, Memorial University, St. John's, NL, A1B 3X7, Canada.*
[b] *Laboratoire Chimie Physique – CLIO, Batiment 201, Porte 2, Campus Universite d'Orsay, 91405 France.*
* tfridgen@mun.ca.
Electronic Supplementary Information (ESI) available: [details of any supplementary information available should be included here]. See DOI: 10.1039/x0xx00000x

lower pH though, the i-motif is quite stable and is predicted to have a dissociation energy of 172 kJ mol $^{-1}$ and a 6.7 kJ mol^{-1} proton transfer barrier between the two cytosines.[24] The i-motif has been found in the regulation regions and telomeres of human cells[25] and it plays a key role in regulating gene expression *in vivo*.

It has been shown [26–28] that methyl group substitution donates more electrons to certain sites of nucleobases which can affect the proton or electron affinity. For example, the proton affinity of the N3 and O2 sites of cytosine are predicted to be practically the same whereas methyl substitution at N1 enhances the proton affinity of the N3 site.[29] Infrared multiple photon dissociation (IRMPD) spectroscopy has been used to confirm the structure of the protonated dimers of both cytosine and 1-methylcytosine shown in Scheme 1 b).[26,30]

The effect of metal cations on i-motif DNA has been studied for several years and depends on metal cation concentration and solution temperature.[31] In their interactions with nucleobases, metal cations can destroy the normal hydrogen bond,[32] can induce stronger interactions,[33] and as well as tautomerization.[34,35] In fact, metal cations are considered as a main cause of mutations in DNA.[36,37] Uracil, for example, has been shown, both theoretically and experimentally, to be most stable as an imide tautomer when interacting with some metal cations.[35,38–41]

Besides the biological interest in i-motifs, it has been studied for its potential to develop materials, such as nanowires, DNA supermolecular hydrogels and DNA motors due to its sensitivity to pH.[42–44] . In the gas phase, the alkali metal cations lithium, sodium, and potassium-bound dimer of cytosine have been studied and compared to the protonated, Cu^+, and Ag^+ bound dimers.[45] The results show that the lowest energy structures for the three alkali metal cation-coordinated dimers of cytosine are tetra-dentate, with the metal cations bound to N3 and O2 of both cytosines, and are of planar symmetric anti-parallel (SAP) geometry as shown in scheme 1(c). The Cu^+ bound dimer, on the other hand, is bi-coordinate—bound to N3 of each cytosine and is similar in geometry to the protonated dimer of cytosine Scheme 1(b).

In this work, the alkali metal cationized 1-methylcytosine (1-mCyt) dimers, $(1\text{-mCyt})_2M^+$ (M=Li, Na, K, Rb, and Cs), were examined in gas phase by infrared multiple photon dissociation (IRMPD) spectroscopy in both the 1000 - 1800 cm^{-1} and 2800 - 3800 cm^{-1} regions. The methylation of cytosine in the 1 position blocks the site attached to ribose/deoxyribose in DNA/RNA. Electronic structure calculations are compared to the gas-phase experimental spectra. A comparison of thermodynamic stability between $(1\text{-mCyt})_2M^+$ structures is provided by computational methods.

2. Methods

2.1 Computational Methods

B3LYP density functional theory has been used to reliably model bioorganic and bioinorganic systems with hydrogen bonds successfully.[46] Geometry optimizations and frequency calculations were performed using the Gaussian 16 (G16) suite of programs[47] using B3LYP density functional theory and the 6-31+G(d,p) split-valence basis set for all atoms except Rb and Cs for which the Def2SVP basis set and relativistic core potential was employed. Single point energy calculations for all optimized structures were performed using B3LYP/6-311+G(3df,3pd) on all atoms except for Rb and Cs for which Def2TZVP was used. For all B3LYP calculations, an empirical dispersion correction was done using Grimme's D3 version with the original D3 damping function, B3LYPD3.[48] M06-2X[49,50] is also considered to be highly reliable for the gas-phase ionic biomolecules with intramolecular interactions. Thus, calculations using the M06-2X method with the 6-31+G(d,p) (Def2SVP on Rb and Cs) were also performed to compare with the B3LYP thermochemical results. The computed IR spectra were scaled by 0.97 and 0.945 in the lower (900-2000 cm^{-1}) and higher (2800-3800 cm^{-1}) energy regions, respectively[51–53], and convoluted with a Lorentzian profile with a width (FWHM) of 15 cm^{-1} to compare with the experimental IRMPD spectra. The relative 298 K Gibbs energies and enthalpies for structures were compared. Reported dissociation energies were corrected for BSSE using the counterpoise correction in G16.

2.2 Experimental Methods.

A Bruker Apex-Qe 7 Fourier-transform ion cyclotron resonance mass spectrometer (FT-ICR-MS) with an Apollo II electrospray ion source was used for all experimental work. To conduct IRMPD spectroscopy in the fingerprint region, the FT-ICR-MS was coupled to a free electron laser (FEL) at the Centre Laser Infrarouge d'Orsay (CLIO).[54] The ions of interest were first mass selected and then irradiated for between 1 and 2 s. The FEL was scanned at 5 cm^{-1} intervals from 900 cm^{-1} to 2000 cm^{-1}. In the 2800 – 3800 cm^{-1} region, IRMPD experiments were conducted in the Laboratory for the Study of Energetics, Structures, and Reactions of Gaseous Ions at Memorial University,[18] where the isolated ions were irradiated with an optical parametric oscillator/amplifier (OPO/A, LaserSpec, 1 W max power) for 2 s. The OPO/A was scanned from 3800 to 2800 cm^{-1} with a 2 cm^{-1} stepsize. The IRMPD efficiencies (ie. infrared intensities) are the negative of the logarithm of the precursor ion intensities divided by the sum of the precursor and product ion intensity.
1-mCyt and alkali metal chlorides were purchased from Sigma-Aldrich and used without further purification. The solution producing the 1-methylcytosine dimers was 1.3 mmol L^{-1} in 1-methylcytosine in 50/50 water/methanol. In 1 mL of this solution 1-2 drops of 10 mmol L^{-1} metal chloride solution was added. Solutions were injected using a 1 mL syringe at a flow rate of 0.15 mL h^{-1}. The temperature of the dry gas was set as 200 ^{o}C.

3. Results and Discussion

3.1 Computed Structures for $(1\text{-mCyt}_2)M^+$

Previous studies have shown that the 1:1 complexes between alkali metal cations and cytosine exist as bidentate structures with the metal cation bound to the carbonyl oxygen and N3 of cytosine in its canonical (keto/amine) form.[34,55] The B3LYP/6-31+G(d,p) calculations on $(1\text{-mCyt})_2M^+$ resulted in only one structure for M=Li, and two each for M=Na, K, Rb, and Cs. These

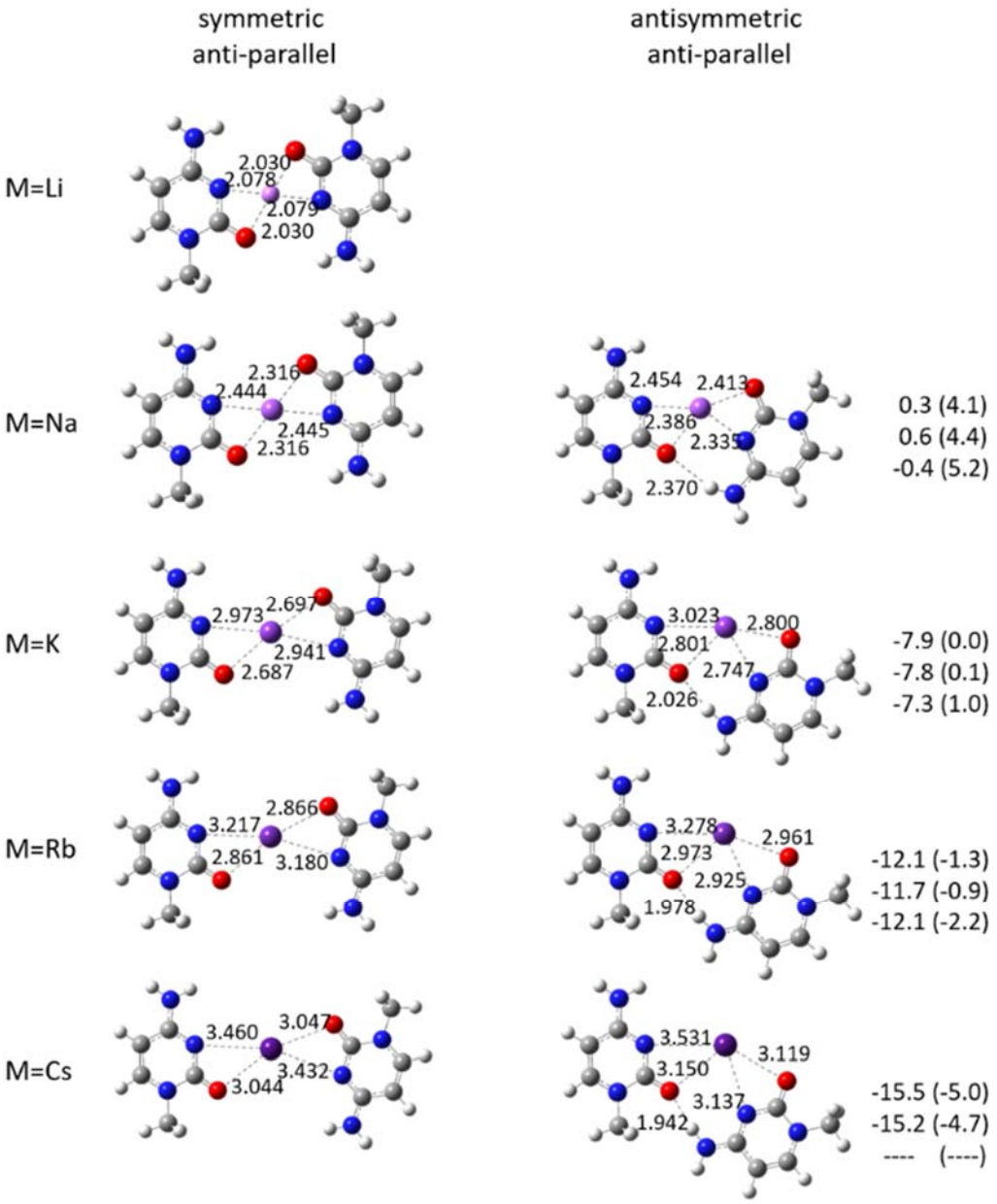

Figure 1. B3LYP/6-31+G(d,p) computed structures for the SAP and AAP structures for (1-mCyt)2M+ complexes. The 298 K enthalpies and Gibbs energies (parentheses) of the AAP structures relative to the SAP structures are also provided at the B3LYPD3/6-31+G(d,p) level (top), B3LYPD3/6-311+G(3df, 3pd)//B3LYPD3/6-31+G(d,p) (middle), and M06-2X/6-31+G(d,p) level (bottom).

structures are shown in Figure 1 with the bond lengths of all electrostatic interactions. The first type of structure, and the only one for M=Li, is a symmetric anti-parallel (SAP) structure in the terminology used previously[45] and can be seen in Figure 1. The SAP structures for $(1\text{-mCyt})_2Li^+$ and $(1\text{-mCyt})_2Na^+$ are fairly symmetric (virtually C_{2h} symmetry), but those for $(1\text{-mCyt})_2K^+$, $(1\text{-mCyt})_2Rb^+$, and $(1\text{-mCyt})_2Cs^+$ are distorted by a slight rotation about the metal cation; the term SAP will still be used for these complexes. In all cases, the SAP structures are tetradentate and, like the 1:1 alkali metal:cytosine complexes mentioned above, are bound to N3 and the carbonyl oxygen of both 1-mCyt. The second structure found for all complexes except $(1\text{-mCyt})_2Li^+$ is similar to the SAP structure except that they are significantly distorted, rotated around the metal cation, so as to allow for a hydrogen bond between the amine group of one 1-mCyt and the carbonyl of the other. This asymmetric anti-parallel (AAP) structure is also tetradentate. As might be expected, as the central ion increases in size and the ion-dipole interaction with cytosine weakens, the structures can distort more easily to form shorter (and stronger) ionic hydrogen bonds to help stabilize the structure.

Note that no other structures involving the keto/amine tautomer were found. Attempts to optimize a non-planar, or planar parallel structure resulted in optimization to the AAP structures.

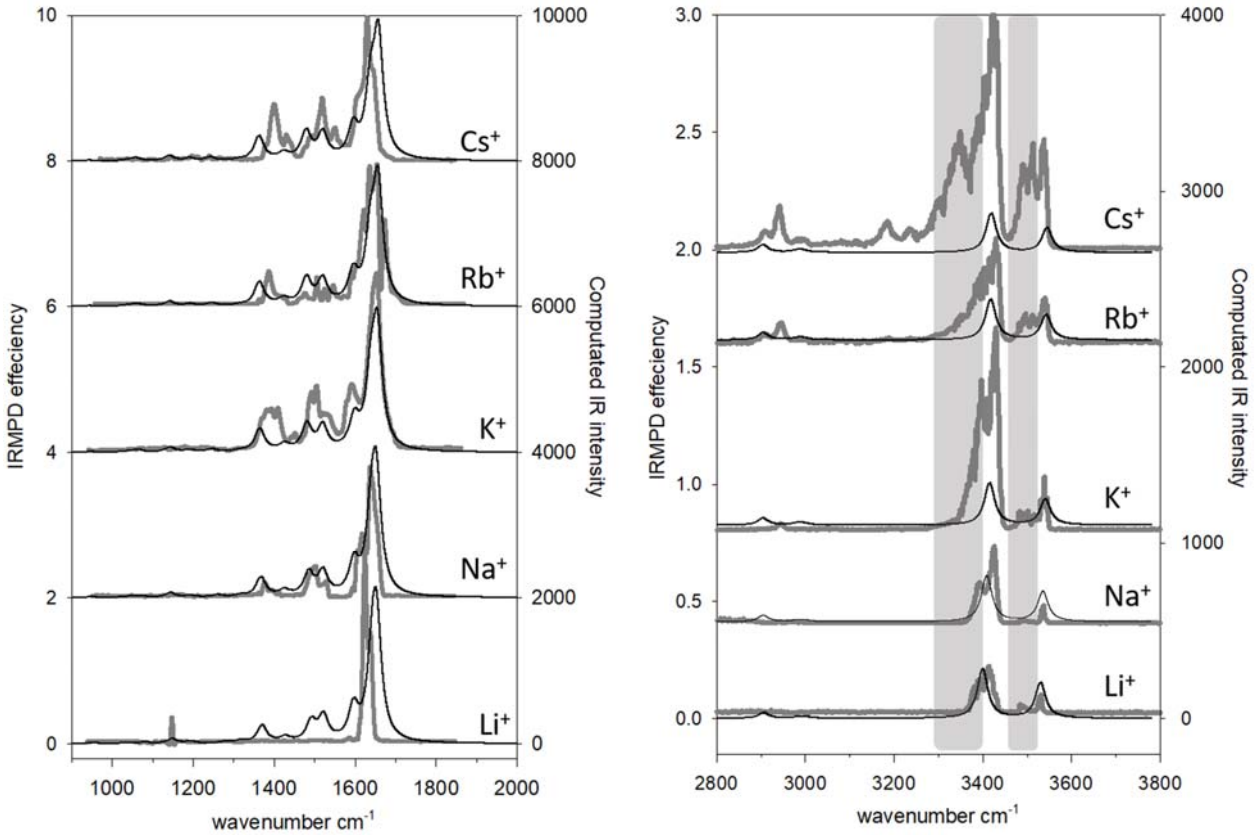

Figure 2. Experimental IRMPD spectra of $(1\text{-mCyt})_2M^+$ complexes, where M= Li^+, Na^+, K^+, Rb^+, Cs^+ (grey traces) and computed IR spectra for the SAP complexes (black traces).

The relative 298 K enthalpies and Gibbs energies of the complexes are also compared in Figure 1 using three different computational methods: B3LYPD3/6-31+G(d,p) (top), B3LYPD3/6-311+G(3df,3pd)// B3LYPD3/6-31+G(d,p) (middle), and M06-2X/6-31+G(d,p) (bottom). For $(1\text{-mCyt})_2Li^+$ and $(1\text{-mCyt})_2Na^+$, the SAP structures are the lowest in Gibbs energy and would be expected to be observed, in fact the AAP conformer is not expected to exist, based on this theory, for the Li^+ complex. For $(1\text{-mCyt})_2K^+$, the SAP and AAP structures are basically isoenergetic in terms of Gibbs energy. For $(1\text{-mCyt})_2Rb^+$ and $(1\text{-mCyt})_2Cs^+$, the AAP structures are favoured. As the metal cation increases in size, the ion-cytosine interaction—which is predominantly an ion-dipole interaction—decreases in strength and the structure-stabilizing hydrogen bonding interaction becomes favoured. Note that for the M06-2X/6-31+G(d,p) calculations, the SAP structure of $(1\text{-mCyt})_2Cs^+$ minimized to a first order transition state with a small imaginary frequency. All attempts to get rid of the imaginary frequency were unsuccessful.

3.2 Vibrational (IRMPD) spectra of $[(1\text{-mCyt})_2M]^+$

Upon absorption of multiple infrared photons resonant with a vibrational mode, all $(1\text{-mCyt})_2M^+$ complexes fragmented by losing a neutral 1-mCyt.

The experimental spectra are compared with the computed IR spectra for the SAP structures in Figure 2. The experimental spectra for all $(1\text{-mCyt})_2M^+$ in the fingerprint region are all quite similar exhibiting metal-coordinated C=O stretching and NH_2 bending between 1600 and 1700 cm^{-1} as well as complex C-C/C-N stretching of the ring and the appendages centred at about 1400 and 1500 cm^{-1}. The computed IR spectra for the SAP structures agree very well with the experimental spectra in the fingerprint region. It is worth mentioning that due to the stronger bonding for $(1\text{-mCyt})_2Li^+$, the photofragment yield is significantly reduced that for the other complexes resulting only one observed band just above 1600 cm^{-1}.

In the higher energy region, bands at 3540 and 3430 cm^{-1} can be ascribed to the NH_2 asymmetric and symmetric stretching modes, respectively, and the computed spectra for the SAP structures reproduce these observed features. On the low energy side of these bands, there are also very weak absorptions or shoulders observed for the $(1\text{-mCyt})_2Li^+$ and $(1\text{-mCyt})_2Na^+$ that broaden and grow to prominence for the $(1\text{-mCyt})_2K^+$, $(1\text{-mCyt})_2Rb^+$, and $(1\text{-mCyt})_2Cs^+$ complexes. It should be noted that a splitting of the asymmetric absorption was also observed for the $(Cyt)_2M^+$ (M=Li, Na, K) complexes.[45]

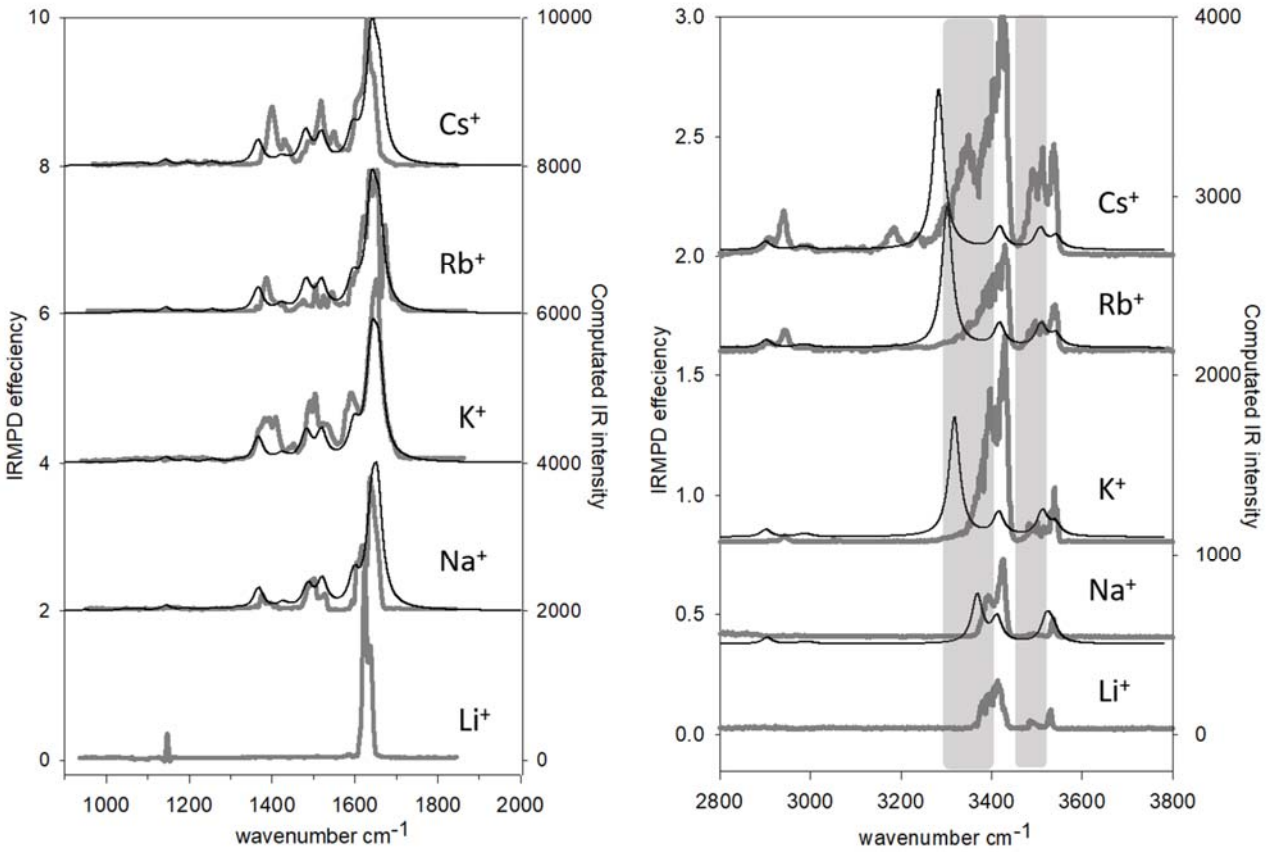

Figure 3. Experimental IRMPD spectra of $(1\text{-mCyt})_2M^+$ complexes, where M= Li^+, Na^+, K^+, Rb^+, Cs^+ (grey traces) and computed IR spectra for the AAP complexes (black traces).

Since there are two NH_2 groups, one for each 1-mCyt, there are in phase and out of phase modes for each of the symmetric and asymmetric stretches. These might be considered the carriers for the shoulders observed—at least the weak ones for $(1\text{-mCyt})_2Li^+$ and $(1\text{-mCyt})_2Na^+$—since none of the complexes are completely symmetric. However, these bands are computed to be nearly degenerate, ranging from as little as 0.2 cm^{-1} to as much as 1.2 cm^{-1} difference for the more asymmetric SAP complexes of $(1\text{-mCyt})_2Cs^+$.

In Figure 3, the experimental spectra are compared to the computed IR spectra for the AAP structures of the $(1\text{-mCyt})_2M^+$complexes. The predicted spectra for the fingerprint region are virtually identical for the SAP (Fig. 2) and AAP (Fig. 3) isomers which are both in very good agreement with the experimental spectra. The similarity in position of the C=O stretching band for the SAP and AAP structures is surprising since there is a significant hydrogen bond in the AAP structures which would lead one to expect a red shift. However, concurrent with the addition of the hydrogen bonding interaction is a lengthening, and presumably weakening, of the C=O--M^+ bond by approximately 0.1 angstrom. This weakening of the C=O--M^+ bond would counteract any expected redshift due to the addition hydrogen bond.

In the higher energy region, due to the hydrogen bonding interactions, the computed in phase and out of phase NH_2 stretching modes are no longer degenerate. The hydrogen bonded symmetric and asymmetric NH_2 stretches are shifted significantly to the red. These hydrogen bonded NH_2 stretching vibrations of the AAP complexes explain the observed low

Table 1. Computed 298 K energetics of dissociation (B3LYP/6-311+G(3df,3pd)//B3LYP/6-31+G(d,p)) for the $(1\text{-mCyt})_2M^+$ complexes. Counterpoise corrections for BSSE are included.

complex	$\Delta_{diss}H^o$ / kJ mol^{-1}	$\Delta_{diss}G^o$ / kJ mol^{-1}
SAP_Li	184.2	144.0
SAP_Na	159.3	122.2
AAP_Na	158.5	117.6
SAP_K	123.3	86.6
AAP_K	130.7	86.2
SAP_Rb	112.4	80.9
AAP_Rb	123.4	81.1
SAP_Cs	99.7	69.3
AAP_Cs	114.6	73.7

energy shoulders that broaden and red shift as the metal gets larger, and the hydrogen bonding interaction gets stronger. That the computed hydrogen bonded NH_2 stretching vibrations do not accurately reproduce the experimental spectra is due to the anharmonicity of the hydrogen bonded N-H stretching and the harmonic nature of the calculations; this has been well documented. [56–61]

The computed relative energetics provided in Fig. 1 (computed dissociation energies are provided in Table 1) are also in agreement with the experimentally observed spectra. Based on the computed energies, we would expect to predominantly observe the SAP complexes for $(1\text{-mCyt})_2Li^+$ and $(1\text{-mCyt})_2Na^+$, whereas we would expect to see both SAP and AAP structures for $(1\text{-mCyt})_2K^+$. For $(1\text{-mCyt})_2Rb^+$ and $(1\text{-mCyt})_2Cs^+$ we would expect to see predominantly the hydrogen bonded AAP structures, although we cannot rule out the existence of the SAP structures neither spectroscopically nor based on the computed energies. However, it is clear that the hydrogen bonded structures are a significant presence for M=K, Rb, and Cs, but not for M=Li and Na.

3.3 Comparison of $(1\text{-mCyt})_2M^+$ and $(Cyt)_2M^+$

In the study by Gao et al.[45] on $(Cyt)_2M^+$ where M=Li, Na and K, it was concluded that only the SAP structures exist as there was no evidence for hydrogen bonded structures. This contrasts the results here that show the $(1\text{-mCyt})_2M^+$ complexes where M=K, Rb, and Cs that clearly show hydrogen bonding AAP structures. Computations on the SAP and AAP structures of $(Cyt)_2M^+$ (M= Na, K, Rb and Cs) were performed and the results are in Table 2.

Table 2. The 298 K relative enthalpies and Gibbs energies, in kJ mol^{-1}, of the cytosine dimeric complexes by three different computational methods.

	B3LYPD3/ 6-31+G(d,p)		B3LYPD3/ 6-311+G(3df,3pd)		M06-2X/ 6-31+g(d,p)	
	$\Delta_{rel}H^o$	$\Delta_{rel}G^o$	$\Delta_{rel}H^o$	$\Delta_{rel}G^o$	$\Delta_{rel}H^o$	$\Delta_{rel}G^o$
SAP_Na	0.0	0.0	0.0	0.0	0.0	0.0
AAP_Na	0.1	5.6	0.8	6.4	-0.9	5.0
SAP_K	0.0	0.0	0.0	0.0	0.0	0.0
AAP_K	-7.7	1.6	-7.4	2.2	-8.0	2.4
SAP_Rb	0.0	0.0	0.0	0.0	0.0	0.0
AAP_Rb	-11.9	0.3	-11.0	1.2	-12.6	-7.3
SAP_Cs	0.0	0.0	0.0	0.0	0.0	0.0
AAP_Cs	-14.9	-2.8	-14.0	-1.9	-15.9	-8.6

Like for the $(1\text{-mCyt})_2Li^+$ complex, only the SAP structure was optimized and attempts to find an AAP structure for $(Cyt)_2Li^+$ were unsuccessful. For the rest of the complexes, the B3LYP calculations predict that only for $(Cyt)_2Cs^+$ is the AAP structure slightly predominant in terms of Gibbs energy, while for $(Cyt)_2K^+$ and $(Cyt)_2Rb^+$, the SAP structure is predicted to be lower in energy, but only slightly. For the M06-2X calculations, the AAP structures are lower in energy for both $(Cyt)_2Rb^+$ and $(Cyt)_2Cs^+$. These calculations are consistent with the observations that no hydrogen bonded structures exist for $(Cyt)_2Li^+$, $(Cyt)_2Na^+$, and $(Cyt)_2K^+$. It should be noted, however, that for the $(Cyt)_2K^+$ IRMPD spectra,[45] there are diffuse shoulders observed that extend to lower energy from both the symmetric and asymmetric stretching bands compared to the $(Cyt)_2Li^+$ and $(Cyt)_2Na^+$ IRMPD spectra.

4. Conclusions

IRMPD spectroscopy in the fingerprint and the higher energy N-H stretching region was used to probe the structures of alkali metal cation bound 1-methylcytosine (1-mCyt) dimers. A comparison of these spectra with computed IR spectra showed that for $(1\text{-mCyt})_2K^+$, $(1\text{-mCyt})_2Rb^+$, and $(1\text{-mCyt})_2Cs^+$, broad shoulders extend from the low energy side of the symmetric and asymmetric NH_2 stretching bands. This broadening is explained as being attributed to hydrogen bonding between the amine group of one cytosine and the carbonyl oxygen of the other cytosine. Evidence for hydrogen bonding interactions were not observed for $(1\text{-mCyt})_2Li^+$ or $(1\text{-mCyt})_2Na^+$. The IRMPD spectra compare very well with the computed IR spectra and the observed results are consistent with the computed energetics between the hydrogen bonded and non-hydrogen bonded complexes. The lowest energy structures for the 1-mCyt complexes were compared to previously studied cytosine complexes $(Cyt)_2M^+$ where M = Li, Na, and K. The calculationed energetics are in agreement that only the non-hydrogen bonded structures would be observed for these cytosine complexes. However, the IRMPD spectrum for $(Cyt)_2K$, does display broadened N-H bands extending to lower energy from both the symmetric and asymmetric stretching bands compared to the $(Cyt)_2Li^+$ and $(Cyt)_2Na^+$ IRMPD spectra;[45] this could indicate that the hydrogen bonding complexes (AAP structures) do exist for $(Cyt)_2K^+$ as they do here for $(1\text{-mCyt})K^+$.

Acknowledgements

The CLIO staff are gratefully acknowledged for their help in obtaining IRMPD spectra in the fingerprint region. The authors acknowledge the computational resources provided by Compute Canada for these studies. The authors also wish to thank the financial contributions from NSERC, CFI, and Memorial University.

Conflicts of interest

There are no conflicts to declare.

References

1 J. R. Williamson, M. K. Raghuraman and T. R. Cech, *Cell*, 1989, **59**, 871–880.
2 D. Bhattacharyya, G. Mirihana Arachchilage and S. Basu, *Front. Chem.*, 2016, **4**, 38.
3 J. T. Davis, *Angew. Chemie - Int. Ed.*, 2004, 43, 668–698.
4 S. N. Georgiades, N. H. A. Karim, K. Suntharalingam and Ramon Vilar, *Angew. Chemie. Int. Ed.*, 2010, **49**, 4020–4034.
5 Y. Wang and D. J. Patel, *Structure*, 1993, **1**, 263–282.
6 C. W. Greider and E. H. Blackburn, *Cell*, 1985, **43**, 405–413.
7 M. L. Bochman, K. Paeschke and V. A. Zakian, *Nat. Rev. Genet.*, 2012, **13**, 770–780.
8 S. Burge, G. N. Parkinson, P. Hazel, A. K. Todd and S. Neidle, *Nucleic Acids Res.*, 2006, **34**, 5402–5415.
9 Y. Wang and D. J. Patel, *Biochemistry*, 1992, **31**, 8112–8119.
10 B. Lippert, *J. Chem. Soc., Dalt. Trans.*, 1997, 3971–3976.
11 W. I. Sundquist and A. Klug, *Lett. to Nat.*, 1989, **342**, 825–829.
12 J. R. Williamson, *Annu. Rev. Biophys. Biomol. Struct.*, 1994, **23**, 703–730.
13 F. W. Smith and J. Feigon, *Nature*, 1992, **356**, 164–168.
14 R. Hänsel-Hertsch, M. Di Antonio and S. Balasubramanian, *Nat. Rev. Mol. Cell Biol.*, 2017, **18**, 279–284.
15 K. Fukushima and H. Iwahashi, *Chem. Commun.*, 2000, 895–896.
16 M. Azargun and T. D. Fridgen, *Phys. Chem. Chem. Phys.*, 2015, **17**, 25778–25785.
17 F. Zaccaria, G. Paragi and C. Fonseca Guerra, *Phys. Chem. Chem. Phys.*, 2016, **18**, 20895–20904.
18 M. Azargun, Y. Jami-Alahmadi and T. D. Fridgen, *Phys. Chem. Chem. Phys.*, 2017, **19**, 1281–1287.
19 G. S. Withers, M. D. Zoback, R. Apel, J. Baumgarter, M. Brudy, R. Emmermann, B. Engeser, K. Fuchs, W. Kessels, H. Rischmuller, F. Rummel and L. Vernlk, *Nat. Lett.*
20 C. Kang, I. Berger, C. Lockshin, R. Ratliff, R. Moyzis, C. Kang, I. Berger, C. Lockshin, R. Ratlifft, R. Moyzist and A. Rich, 1994, **91**, 11636–11640.
21 M. Guéron and J. L. Leroy, *Curr. Opin. Struct. Biol.*, 2000, **10**, 326–331.
22 A. T. Phan and J.-L. Mergny, *Nucleic Acids Res.*, 2002, **30**, 4618–4625.
23 S. Benabou, A. Aviñó, R. Eritja, C. González and R. Gargallo, *RSC Adv.*, 2014, **4**, 26956–26980.
24 S. Y. Han and H. Bin Oh, *Chem. Phys. Lett.*, 2006, **432**, 269–274.
25 M. Zeraati, D. B. Langley, P. Schofield, A. L. Moye, R. Rouet, W. E. Hughes, T. M. Bryan, M. E. Dinger and D. Christ, *Nat. Chem.*, 2018, **10**, 631–637.
26 B. Yang, A. R. Moehlig, C. E. Frieler and M. T. Rodgers, *J. Phys. Chem. A*, 2015, **119**, 1857–1868.
27 C. Desfrançois, H. Abdoul-Carime, V. P. S. Carles, J. P. Schermann, D. M. A. Smith and L. Adamowicz, *J. Chem. Phys.*, 1999, **110**, 11876.
28 M. Etinski and C. M. Marian, *Phys. Chem. Chem. Phys.*, 2009, **12**, 4915–4923.
29 M. Liu, T. Li, F. S. Amegayibor, D. S. Cardoso, Y. Fu and J. K. Lee, *J. Org. Chem.*, 2008, **73**, 9283–9291.
30 J. Oomens, A. R. Moehlig and T. H. Morton, *J. Phys. Chem. Lett.*, 2010, **1**, 2891–2897.
31 A. Ono, H. Torigoe, Y. Tanaka and I. Okamoto, *Chem. Soc. Rev.*, 2011, **40**, 5855–5866.
32 S. Menzer, M. Sabat and B. Lippert, *J. Am. Chem. Soc.*, 1992, **114**, 4644–4649.
33 M. H. Shamsi and H. B. Kraatz, *J. Inorg. Organomet. Polym. Mater.*, 2013, **23**, 4–23.
34 M. Kabeláč and P. Hobza, *J. Phys. Chem. B*, 2006, **110**, 14515–14523.
35 R. Cheng, V. E. Rose, B. Power and T. D. Fridgen, *Phys. Chem. Chem. Phys.*, 2017, **20**, 572–580.
36 G. L. Eichhorn, N. A. Berger, J. J. Butzow, P. Clark, J. Heim, J. Pitha, C. Richardson, J. M. Rifkind, Y. Shin and E. Tarien, in *Metal Ions in Biological Systems*, ed. S. K. Dhar, Springer US, Boston, MA, 1973, pp. 43–66.
37 B. Lippert, *J. Chem. Soc. Dalt. Trans.*, 1997, **21**, 3971–3976.
38 E. a. L. Gillis, M. Demireva, K. Nanda, G. Beran, E. R. Williams and T. D. Fridgen, *Phys. Chem. Chem. Phys.*, 2012, **14**, 3304.
39 K. J. Koch, T. Aggerholm, S. C. Nanita and R. G. Cooks, *J. Mass Spectrom.*, 2002, **37**, 676–686.
40 J. M. Bakker, R. K. Sinha, T. Besson, M. Brugnara, P. Tosi, J. Y. Salpin and P. Maître, *J. Phys. Chem. A*, 2008, **112**, 12393–12400.
41 E. L. Zins, S. Rochut and C. Pepe, *J. Mass Spectrom.*, 2009, **44**, 40–49.
42 P. Alberti, A. Bourdoncle, B. Saccà, L. Lacroix and J. L. Mergny, *Org. Biomol. Chem.*, 2006, **4**, 3383–3391.
43 D. Liu and S. Balasubramanian, *Angew. Chemie - Int. Ed.*, 2003, **42**, 5734–5736.
44 Y. Dong, Z. Yang and D. Liu, *Acc. Chem. Res.*, 2014, **47**, 1853–1860.
45 J. Gao, G. Berden, M. T. Rodgers and J. Oomens, *Phys. Chem. Chem. Phys.*, 2016, **18**, 7269–7277.
46 M. Meyer, T. Steinke, M. Brandl, J. Sühnel and M. E. T. Al, 2000, **22**, 109–124.
47 M. H. M. J. Frisch, G. W. Trucks, H. B. Schlegel, G. E. Scuseria, M. A. Robb, J. R. Cheeseman, G. Scalmani, V. Barone, B. Mennucci, G. A. Petersson, H. Nakatsuji, M. Caricato, X. Li, H. P. Hratchian, A. F. Izmaylov, J. Bloino, G. Zheng, J. L. Sonnenberg, *Gaussian, Inc. Wallingford, CT*.
48 S. Grimme, J. Antony, S. Ehrlich and H. Krieg, *J. Chem. Phys.*, 2010, **132**, 154104.
49 M. Walker, A. J. A. Harvey, A. Sen and C. E. H. Dessent, *J. Phys. Chem. A*, 2013, **117**, 12590–12600.
50 E. G. Hohenstein, S. T. Chill and C. D. Sherrill, *Methods*, 2008, **4**, 1996–2000.
51 Y. Jami-Alahmadi and T. D. Fridgen, *Phys. Chem. Chem. Phys.*, 2016, **18**, 2023–2033.
52 B. Power, V. Haldys, J. Y. Salpin and T. D. Fridgen, *Int. J.*

Mass Spectrom., 2015, **378**, 328–335.
53 R. Cheng, V. E. Rose, B. Power and T. D. Fridgen, *Phys. Chem. Chem. Phys.*, 2018, **20**, 572–580.
54 R. Prazeres, F. Glotin, C. Insa, D. A. Jaroszynski and J. M. Ortega, *Eur. Phys. J. D*, 1998, **3**, 87–93.
55 B. Yang, R. R. Wu, N. C. Polfer, G. Berden, J. Oomens and M. T. Rodgers, *J. Am. Soc. Mass Spectrom.*, 2013, **24**, 1523–1533.
56 E. A. L. Gillis and T. D. Fridgen, *Int. J. Mass Spectrom.*, 2010, **297**, 2–8.
57 A. Cimas, T. D. Vaden, T. S. J. A. De Boer, L. C. Snoek and M. Gaigeot, *J. Chem. Theory Comput.*, 2009, **5**, 1068–1078.
58 C. Fraschetti, L. Guarcini, M. Speranza and A. Filippi, *Int. J. Mass Spectrom.*, 2019, **438**, 148–156.
59 B. D. Linford, A. Le Donne, D. Scuderi, E. Bodo and T. D. Fridgen, *Eur. J. Mass Spectrom.*, 2018, **0**, 1–9.
60 M. B. Moghaddam and T. D. Fridgen, *J. Phys. Chem. B*, 2013, **117**, 6157–6164.
61 M. B. Burt and T. D. Fridgen, *J. Phys. Chem. A*, 2013, **117**, 1283–1290.

